Supplementary materials:

Combat biofouling with ridge-like surface morphology: A bioinspired study

Jimin Fu[1], Hua Zhang[1,2], Zhenbin Guo[1], Dan-qing Feng[3], Vengatesen Thiyagarajan[4], Haimin Yao[1,*]

[1]Department of Mechanical Engineering, The Hong Kong Polytechnic University, Hung Hom, Kowloon, Hong Kong SAR, China

[2]Department of Chemistry and Chemical Engineering, Jiangxi Normal University, Nanchang, 330022, China

[3] State-Province Joint Engineering Laboratory of Marine Bioproducts and Technology, College of Ocean and Earth Sciences, Xiamen University, Xiamen 361005, China

[4]The Swire Institute of Marine Sciences and School of Biological Sciences, The University of Hong Kong, Hong Kong SAR, China

[*]Author for correspondence, E-mail: mmhyao@polyu.edu.hk (Haimin Yao)

1. Pull-off forces of different attachment configurations

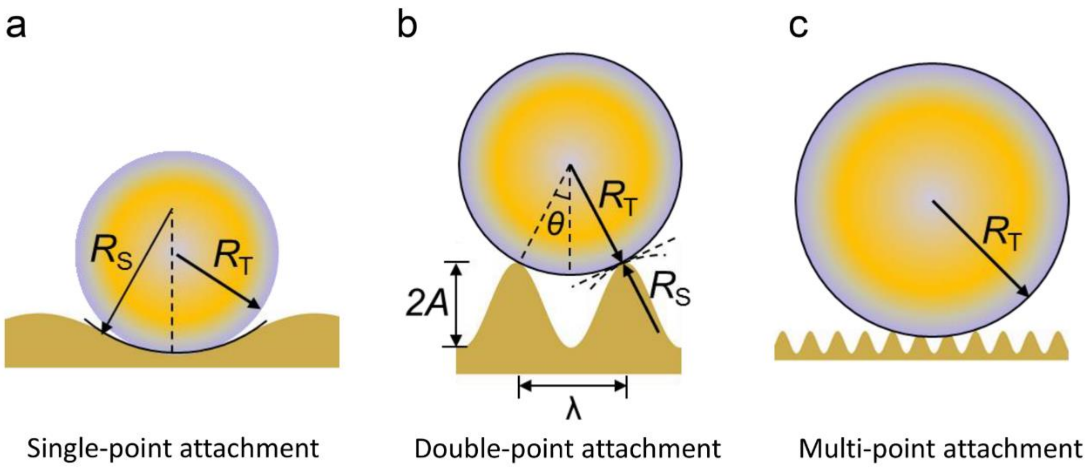

Figure S1. Schematics of three possible attachment configurations of a tubeworm attached on substrate with wavy profile: (a) single-point attachment, (b) double-point attachment and (c) multi-point attachment.

For a substrate with wavy profile, we assume that the profile is periodic and can be described by function $y = -A\cos(2\pi x/\lambda)$, where λ and A denote the wavelength and amplitude, two characteristic length scales of the profile, respectively. There are three distinct attachment configurations, depending on the characteristic length scales of the profile, as shown in figure S1a-c. If the wavelength of the profile λ is much larger than the tubeworm's radius R_{T}, the tubeworm rest at the trough of the groove, as shown in figure S1a. This configuration is called as single-point attachment. For profile with smaller λ, the tubeworm has to straddle over a groove between two adjacent ridges, forming a configuration called double-point attachment (see figure S1b). If λ is much smaller than the size of the tubeworm, more than two contact points will form between the tubeworm and the substrate, giving rise to a multi-point attachment configuration, as shown in figure S1c.

1.1 Pull-off force of single-point attachment configuration

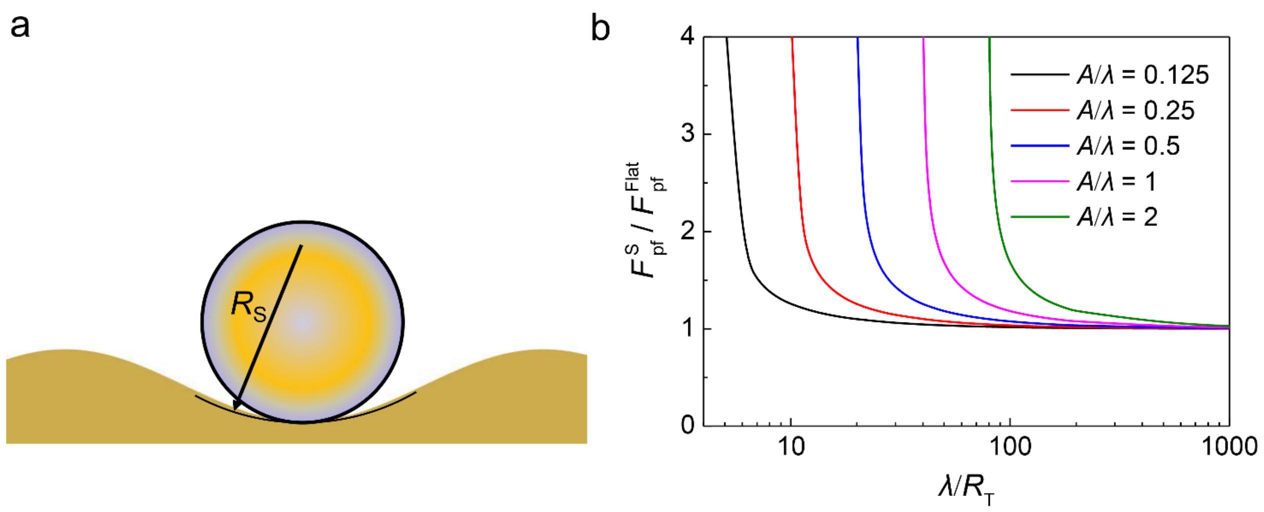

Figure S2. (a) Schematic of single-point attachment configuration. (b). Variation of the pull-off force with λ/R_T for single-point attachment configuration with various A/λ .

In single-point attachment configuration, the cylinder rests on the trough region, as shown in figure S2a, there is only one contact point between the cylinder and the substrate. Earlier studies indicated that the pull-off force to separate two cylindrical bodies is given by [1]

$$F_{pf}^{S} = 3\left(\frac{\pi E^* W^2 R}{16}\right)^{1/3} \tag{S1.1}$$

where $R = \frac{R_S R_T}{R_S + R_T}$, $E^* = 1/\left[\left(1-\nu_T^2\right)/E_T + \left(1-\nu_S^2\right)/E_S\right]$ and W is the work of adhesion. Since pull-off force between a cylinder and a flat substrate is

$$F_{pf}^{Flat} = 3\left(\frac{\pi E^* W^2 R_T}{16}\right)^{1/3}. \tag{S1.2}$$

Equation (S1.1) can be written as

$$F_{\mathrm{pf}}^{\mathrm{S}} = \left(\frac{R_{\mathrm{S}}}{R_{\mathrm{S}} + R_{\mathrm{T}}}\right)^{1/3} F_{\mathrm{pf}}^{\mathrm{Flat}}. \tag{S1.3}$$

Here, R_{T} and R_{S} stand for the radii of curvature of the tubeworm and substrate at the contact point respectively. For a profile defined by function $y = -A\cos\left(\frac{2\pi x}{\lambda}\right)$, the radius of curvature at the trough R_{S} can be calculated by $R_{\mathrm{S}} = -\frac{\left(1 + y'(0)^2\right)^{3/2}}{y''(0)}$, where $y'(0)$ and $y''(0)$ stand for the first and second derivatives of function y at x=0. Thus, R_{S} is given by

$$R_{\mathrm{S}} = -\frac{\lambda^2}{4\pi^2 A}. \tag{S1.4}$$

By inserting equation (S1.4) into (S1.3), the normalized pull-off force for single-point attachment configuration, $F_{\mathrm{pf}}^{\mathrm{S}} / F_{\mathrm{pf}}^{\mathrm{Flat}}$, can be given as a function of λ / R_{T} for a given A/λ. The dependence of $F_{\mathrm{pf}}^{\mathrm{S}} / F_{\mathrm{pf}}^{\mathrm{Flat}}$ on λ / R_{T} for different A/λ is shown in figure S2b. From equation (S1.3) and figure S2b, it can be noticed that $F_{\mathrm{pf}}^{\mathrm{S}}$ goes to infinity when $R_{\mathrm{S}} = -R_{\mathrm{T}}$. Such unrealistic singularity of the predicted pull-off force is essentially attributed to the conventional parabolic approximation for circular profiles in contact mechanics [1], because when $R_{\mathrm{S}} = -R_{\mathrm{T}}$, this result actually describes the pull-off force between a concave surface and a conformal solid with exactly the same parabolic-shaped profile. To overcome this dilemma, we have to estimate an upper limit for $F_{\mathrm{pf}}^{\mathrm{S}}$.

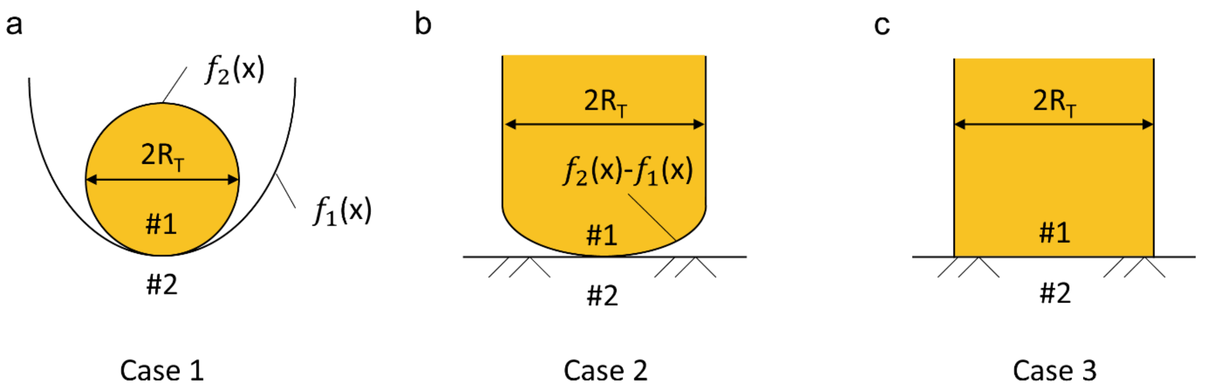

Figure S3. (a) Contact between two solids with profile functions $f_1(x)$ and $f_2(x)$. (b) Contact between a solid with profile function $f_2(x) - f_1(x)$ and a flat substrate. (c) Contact between a solid with flat profile and a flat substrate.

For adhesive contact case between two solid materials with profile functions $f_1(x)$ and $f_2(x)$ (see Figure S3a), it can be demonstrated in contact mechanics that the pull-off force in-between is equal to that of an equivalent case in which one material has profile function $f_2(x)-f_1(x)$ while the other is totally flat (see Figure S3b). Meanwhile, it can be demonstrated that such pull-off force reaches its maximum when the profile is flat, namely $f_2(x)-f_1(x)=0$. This cap value is given by

$$F_{\mathrm{pf}}^{\mathrm{Cap}}=\sqrt{2\pi E^{*}WR_{\mathrm{T}}}\ , \qquad \text{(S2.1)}$$

which can be further expressed in terms of $F_{\mathrm{pf}}^{\mathrm{Flat}}$ as

$$F_{\mathrm{pf}}^{\mathrm{Cap}}=1.19\left(\frac{\pi E^{*}R_{\mathrm{T}}}{W}\right)^{1/6}F_{\mathrm{pf}}^{\mathrm{Flat}}\ . \qquad \text{(S2.2)}$$

Here, the tubeworm larva is assumed as an elastic cylinder with radius $R_{\mathrm{T}}=50\,\mu\mathrm{m}$, and the adhesion system including the larva and the substrate is assumed perfectly bonded with elastic modulus $E^{*}=100\,\mathrm{kPa}$ and work of adhesion $W=0.1\,\mathrm{J/m^2}$. These values taken in the theoretical modeling are close to those in similar natural adhesion systems as shown in Table S1. The cap value can be determined by using equation (S2.2), is around as 2.8 times as $F_{\mathrm{pf}}^{\mathrm{Flat}}$.

Table S1. Typical mechanical properties in natural adhesion systems and the theoretical modeling.

Fouler	Elastic modulus *E*	Work of adhesion *W*
Cell[2-4]	0.1-100 kPa	0.01-10 mJ/m^2
Alga[5, 6]	2-10 MPa	0.01-0.1 J/m^2
Barnacle[7]	0.2- 5 MPa	
Theoretical modeling	100 kPa	0.1 J/m^2

1.2 Pull-off force of double-point attachment configuration

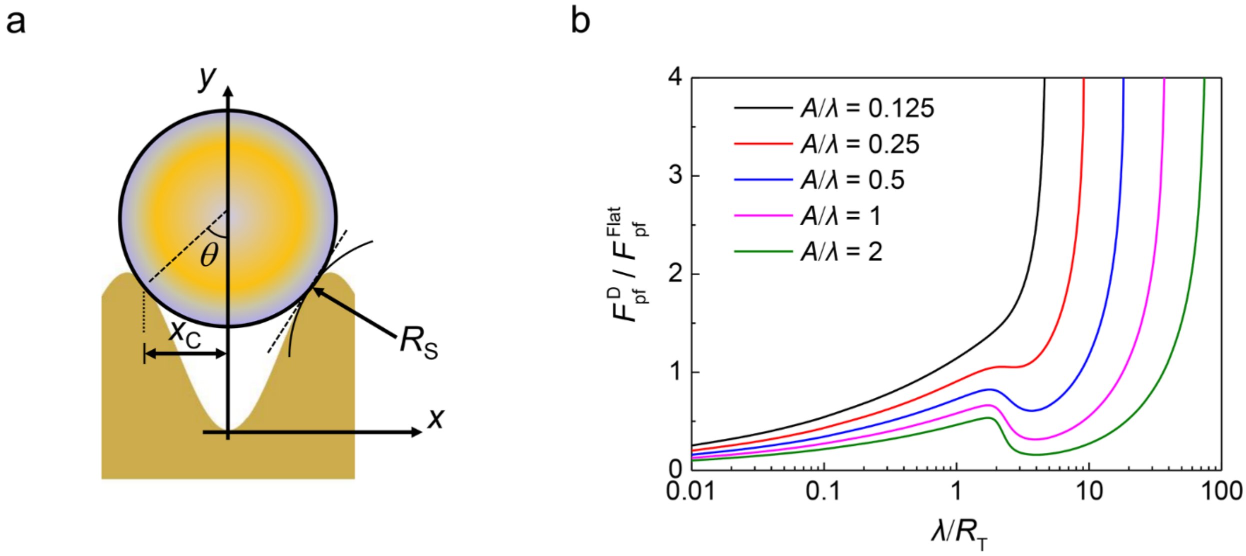

Figure S4. (a) Schematic of double-point attachment configuration. (b). Variation of the pull-off force with λ/R_T for double-point attachment configuration with various A/λ .

For double-point attachment configuration, the cylinder straddles over a groove between two adjacent ridges. The pull-off force equals the resultant force of the adhesion on both contact points

$$F_\mathrm{pf}^\mathrm{D} = 2\cos\theta \cdot F_\mathrm{pf}^\mathrm{ridge}, \tag{S3.1}$$

where $F_\mathrm{pf}^\mathrm{ridge}$ is the pull-off force on one ridge, and θ is the contact angle designated in figure S4a.

For the adhesion with a single ridge, the pull-off force can be written as

$$F_\mathrm{pf}^\mathrm{ridge} = \left(\frac{R_\mathrm{S}}{R_\mathrm{S} + R_\mathrm{T}}\right)^{1/3} F_\mathrm{pf}^\mathrm{Flat}, \tag{S3.2}$$

where R_S is the curvature radius at the contact point of the substrate.

Combining equation (S3.1) and (S3.2), F_pf^D can be rewritten as

$$F_\mathrm{pf}^\mathrm{D} = 2\cos\theta \cdot \left(\frac{R_\mathrm{S}}{R_\mathrm{S} + R_\mathrm{T}}\right)^{1/3} F_\mathrm{pf}^\mathrm{Flat}. \tag{S3.3}$$

The radius of curvature at the contact point R_S can be calculated from the profile function $y(x)$ through

$$R_\mathrm{S} = -\frac{\left(1 + y'^2\right)^{3/2}}{y''}, \tag{S3.4}$$

where the first and second derivatives of the profile function are given by $y' = A \cdot (2\pi/\lambda) \cdot \sin(2\pi x_C/\lambda)$ and $y'' = A \cdot (2\pi/\lambda)^2 \cdot \cos(2\pi x_C/\lambda)$, respectively. In above expressions, x_C presents the coordinate of the contact point in the x direction (see Figure S4a), which can be determined from following geometrical relationship

$$\frac{x_C}{\sqrt{{R_T}^2 - {x_C}^2}} = 2\pi \cdot \left(\frac{A}{\lambda}\right) \cdot \sin\left(\frac{2\pi x_C}{\lambda}\right). \qquad \text{(S3.5)}$$

Therefore, for given A/λ, it can be seen from equation (S3.5) that normalized coordinate x_C/R_T is a function of λ/R_T.

As to the contact angel θ, basic geometric relationship implies that

$$\cos\theta = \sqrt{1 - (x_C/R_T)^2}. \qquad \text{(S3.6)}$$

Equation (S3.6) indicates that for given A/λ, $\cos\theta$ is a function of λ/R_T. Therefore, F_{pf}^{D}/F_{pf}^{Flat} according to equation (S3.3) should be a function of λ/R_T for given A/λ. Figure S4b shows the variation of F_{pf}^{D}/F_{pf}^{Flat} with λ/R_T for different A/λ. As λ/R_T increases, F_{pf}^{D} will approach to F_{pf}^{S} which has singularity when $R_T = -R_S$ or $\lambda/R_T = 4\pi^2 A/\lambda$. This singularity problem has been well addressed above by introducing a reasonable cap for the pull-off force when $R_S = -R_T$.

1.3 Pull-off force of multi-point attachment configuration

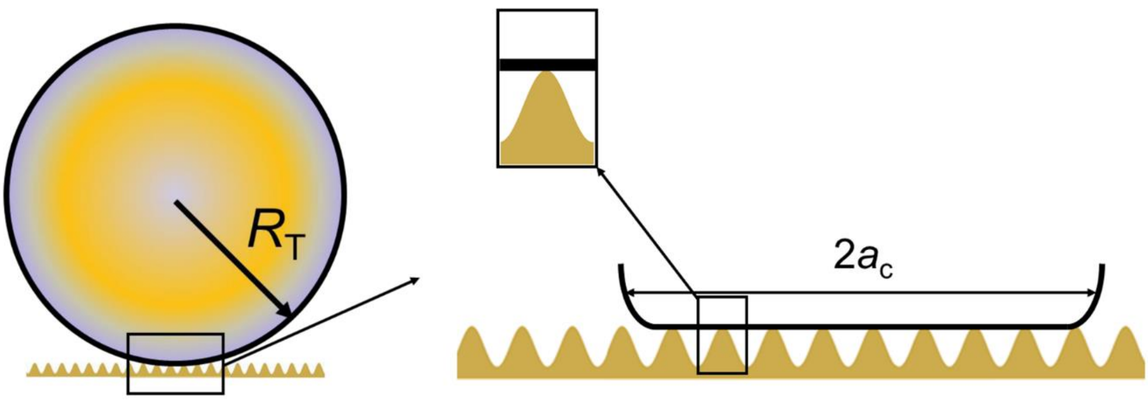

Figure S5. Schematic of multi-point attachment configuration.

With the decrease of the λ, more than two ridges will contact the cylinder, as shown in figure S5. To simplify the problem, the contact at each ridge is assumed identical. Thus, for this multi-point attachment configuration, the pull-off force $F_{\mathrm{pf}}^{\mathrm{M}}$ can be roughly estimated as

$$F_{\mathrm{pf}}^{\mathrm{M}} = N \cdot F_{\mathrm{pf}}^{\mathrm{ridge}} , \tag{S4.1}$$

where N is the number of the ridges in contact with the cylinder, and $F_{\mathrm{pf}}^{\mathrm{ridge}}$ is the pull-off force contributed by one ridge. The number of the ridges N can be estimated from the expression

$$N = \frac{2a_{\mathrm{c}}}{\lambda}, \tag{S4.2}$$

where $2a_{\mathrm{c}}$ is the nominal contact width between the cylinder and the substrate at the pull-off moment, as shown in figure S5, which can be given by

$$2a_{\mathrm{c}} = 2 \cdot \left(\frac{2W_{\mathrm{equ}} R_{\mathrm{T}}^{\ 2}}{\pi E^{*}} \right)^{\frac{1}{3}} \tag{S4.3}$$

where W_{equ} is the equivalent adhesion energy between the cylinder and wavy substrate given by

$$W_{\mathrm{equ}} = \frac{2a_{\mathrm{each}}}{\lambda} \cdot W = \left(\frac{W^{4} \lambda}{\pi^{5} E^{*} A^{2}} \right)^{1/3} . \tag{S4.4}$$

Meanwhile, the pull-off force contributed by one ridge is given by

$$F_{\mathrm{pf}}^{\mathrm{ridge}} = \left(\frac{\lambda^{2}}{4\pi^{2} A R_{\mathrm{T}}} \right)^{\frac{1}{3}} F_{\mathrm{pf}}^{\mathrm{Flat}} . \tag{S4.5}$$

By combining equation (S4.1- 4.5), it can be estimated that

$$F_{\mathrm{pf}}^{\mathrm{M}} = \left(\frac{2}{\pi} \right)^{10/9} \left(\frac{W}{2\pi E^{*} R_{T}} \right)^{4/9} \left(\frac{\lambda}{A} \right)^{5/9} \left(\frac{\lambda}{R_{T}} \right)^{-7/9} \cdot F_{\mathrm{pf}}^{\mathrm{Flat}} . \tag{S4.6}$$

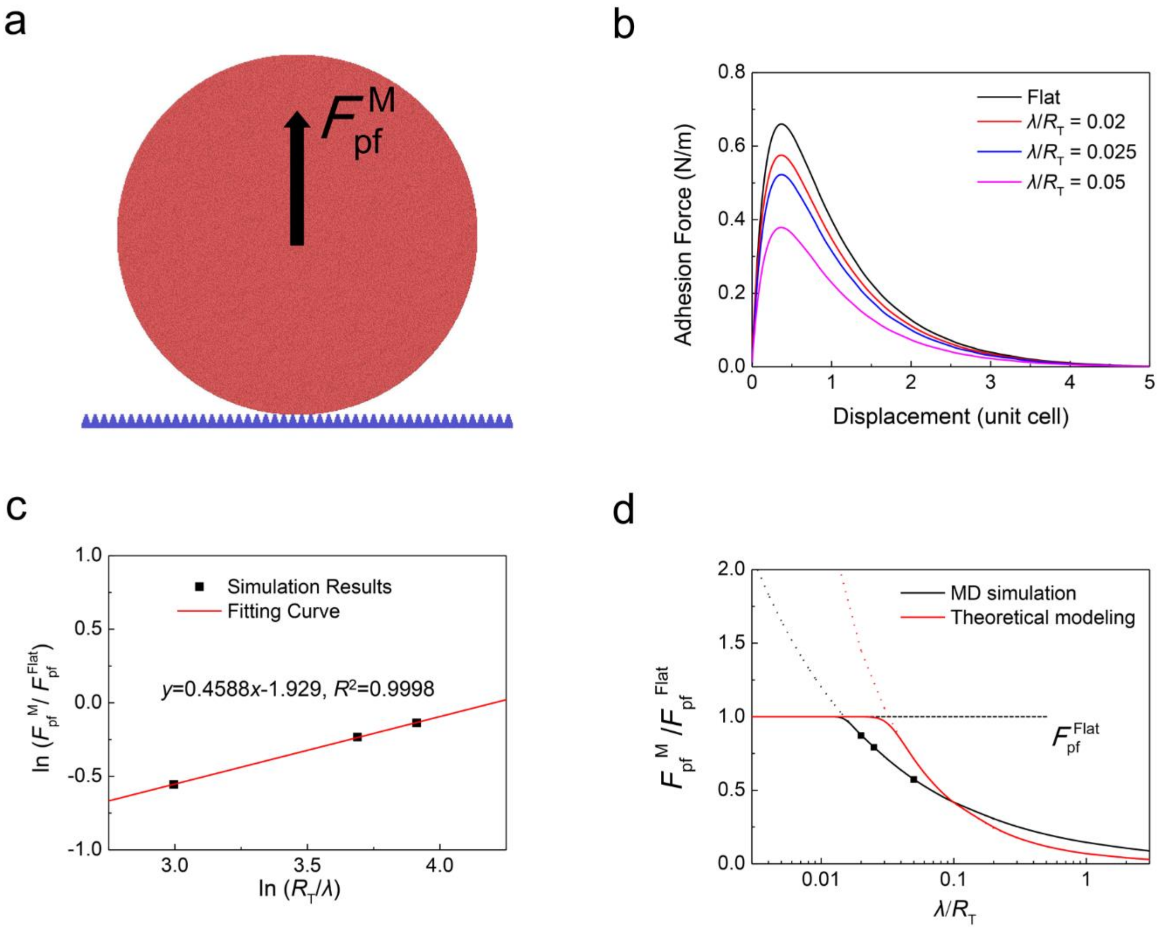

Figure S6. (a) Schematics of the CGMD simulation model. (b). The calculated dependence of the adhesion force on the displacement of the cylinder. (c) Calculated evolution of the normalized pull-off force with ln (R_T/λ). Here A/λ is taken as 0.5. (d) Comparison of calculated normalized pull-off force as a function λ/R_T with the theoretical prediction given by equation (S4.6). For the plot of the theoretical curve, related parameters were taken as the representative values shown in Table S1.

In the derivation of equation (S4.6), the interaction between the adhesions on different ridges is neglected. To shed light on the coupling effect of adjacent adhesion points, coarse grain molecular dynamics (CGMD) simulations were carried out with LAMMPS package [8]. Figure S6a shows the simulation model, in which an elastic cylinder is spontaneously attached onto a sinusoidal substrate and then is pulled off from it at a constant speed. Lennard-Jones (L-J) force field

$U_{\mathrm{LJ}}(r) = 4\varepsilon[(\sigma/r)^{12} - (\sigma/r)^{6}]$ was applied to describe the interactions between the atoms in the system, including the cohesion inside the cylinder and interfacial adhesion between the cylinder and substrate. Due to the limitation of the computation scale in MD simulation, the radius of the cylinder, which was taken as R_{T}=50 μm in our previous theoretical modelling, was set as 400 nm. Equation (S4.6) implies that the effect of such discrepancy in R_{T} on the pull-off force can be compensated as long as $W/E^{*}R_{T}$ remains unchanged. For this purpose, in the L-J potential describing the cohesion in the cylinder, ε and σ were taken as 0.00185 eV and 1.29 nm respectively, giving rise to the effective Young's modulus of the cylinder equal to 12.5 MPa; in the L-J potential describing the interfacial adhesion, ε and σ were taken as 0.33 eV and 2.58 nm respectively, resulting in the adhesion energy W = 0.1 J/m^2. As to the substrate, in addition to the flat benchmark, three sinusoidal profiles with λ/R_{T} equal to 0.02, 0.025 and 0.05 were considered with A/λ being taken as 0.5 always. The substrate was assumed rigid by fixing the displacements of its atoms in all dimensions. In each simulation case, the system was initially relaxed using the canonical ensemble (NVT) for 200 ps. The time step of the simulations was taken as 1 fs and temperature was controlled at 300 K with the Langevin thermostat. Visualization program OVITO [10] was used to visualize and output the simulations results.

Figure S6b shows the evolution of the calculated adhesion force as the cylinder recedes from the substrate. Clearly, the pull-off force, which refers to the maximum adhesion force, depends on λ/R_{T} . By fitting the calculated data points (see Figure S6c), such dependence is found to follow the trend depicted by function of $\ln\left(F_{\mathrm{pf}}^{\mathrm{M}}/F_{\mathrm{pf}}^{\mathrm{Flat}}\right) = 0.4588 \cdot \ln\left(R_{T}/\lambda\right) - 1.929$, which implies

$$F_{\mathrm{pf}}^{\mathrm{M}} = 0.1453 \cdot \left(\frac{\lambda}{R_{\mathrm{T}}}\right)^{-0..4588} F_{\mathrm{pf}}^{\mathrm{Flat}} . \qquad \text{(S4.7)}$$

Nevertheless, both equations (S4.6) and (S4.7) indicate that F_{pf}^{M} will go to infinity as λ approaches zero. This trend is clearly contradictory to the fact that F_{pf}^{M} should asymptotically approach to $F_{\text{pf}}^{\text{Flat}}$ as λ/R_{T} approaches zero. Therefore, it should be the applicable condition of equations (S4.6) and (S4.7) that $F_{\text{pf}}^{\text{M}} \le F_{\text{pf}}^{\text{Flat}}$ or $F_{\text{pf}}^{\text{M}} / F_{\text{pf}}^{\text{Flat}} \le 1$. Figure S6d plots the equation (S4.7) in comparison with equation (S4.6). Both curves exhibit the similar trends as λ/R_{T} increases, implying that equation (S4.6) gives a reasonable estimation to the pull-off force even though the coupling effect is neglected.

2. Culture of the tubeworm larvae for settlement tests

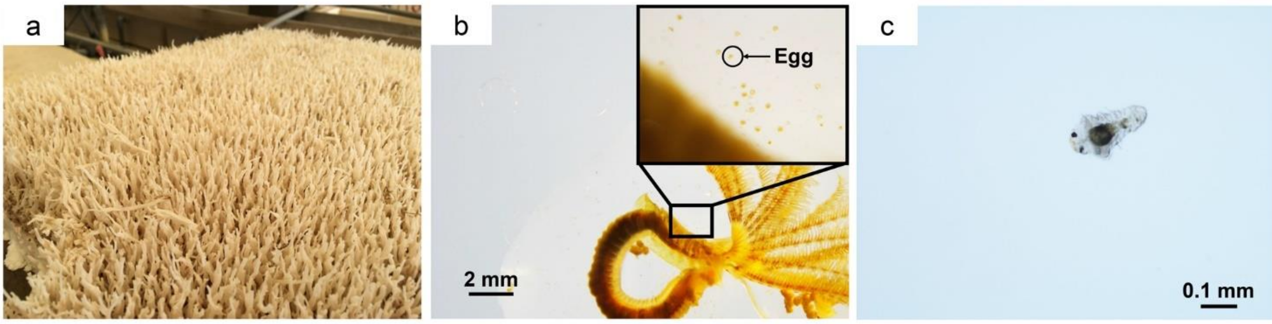

Figure S7. (a) Adult tubeworms *Hydroides elegans* attached on a plastic plate. (b) Adult tubeworm removed from calcified tubular shell. (c) Larval tubeworm swimming in the seawater to detect the target surface for attachment.

Adult tubeworms *H. elegans* (figure S7a) were collected from a bay near Yung Shue O, Hong Kong. After breaking the tubular shells of some tubeworm adults with tweezers, eggs and sperms were released and collected, as shown in figure S7b. Fertilization was carried out by mixing the collected eggs and sperms for 30 min in filtered seawater (with 0.22 μm mesh sized filter) at ambient temperature (25 °C), normal pH value (~8.1) and salinity (34 psu). After fertilization, the embryos were raised at the density of 5 larvae ml^{-1} in the culture tanks for 5-7 days. During this period, the seawater was refreshed every two days and the larvae were fed with algal *Isochrysis galbana* (about 10^5 cells ml^{-1}). The larvae aged 5-7 days (see figure S7c) were ready for attachment tests. To facilitate the settlement on biofilm-free surfaces like our samples, artificial settlement stimuli (CsCl, 5 mmol/L) was applied.

References

[1] Chaudhury, M.K., Weaver, T., Hui, C.Y. & Kramer, E.J. 1996 Adhesive contact of cylindrical lens and a flat sheet. *J. Appl. Phys.* **80**, 30-37. (doi:10.1063/1.362819).

[2] Kuznetsova, T.G., Starodubtseva, M.N., Yegorenkov, N.I., Chizhik, S.A. & Zhdanov, R.I. 2007 Atomic force microscopy probing of cell elasticity. *Micron* **38**, 824-833. (doi:10.1016/j.micron.2007.06.011).

[3] Gavara, N. & Chadwick, R.S. 2012 Determination of the elastic moduli of thin samples and adherent cells using conical atomic force microscope tips. *Nat. Nanotechnol.* **7**, 733-736. (doi:10.1038/nnano.2012.163).

[4] Guo, Q.Q., Xia, Y., Sandig, M. & Yang, J. 2012 Characterization of cell elasticity correlated with cell morphology by atomic force microscope. *J. Biomech.* **45**, 304-309. (doi:10.1016/j.jbiomech.2011.10.031).

[5] Callow, J.A., Callow, M.E., Ista, L.K., Lopez, G. & Chaudhury, M.K. 2005 The influence of surface energy on the wetting behaviour of the spore adhesive of the marine alga Ulva linza (synonym Enteromorpha linza). *J. R. Soc. Interface* **2**, 319-325. (doi:10.1098/rsif.2005.0041).

[6] Walker, G.C., Sun, Y.J., Guo, S.L., Finlay, J.A., Callow, M.E. & Callow, J.A. 2005 Surface mechanical properties of the spore adhesive of the green alga Ulva. *J. Adhes.* **81**, 1101-1118. (doi:10.1080/00218460500310846).

[7] Sun, Y.J., Guo, S.L., Walker, G.C., Kavanagh, C.J. & Swain, G.W. 2004 Surface elastic modulus of barnacle adhesive and release characteristics from silicone surfaces. *Biofouling* **20**, 279-289. (doi:10.1080/08927010400026383).

[8] Plimpton, S. 1995 Fast Parallel Algorithms for Short-Range Molecular-Dynamics. *J. Comput. Phys.* **117**, 1-19. (doi:DOI 10.1006/jcph.1995.1039).

[9] Lin, S., Chen, C.T., Bdikin, I., Ball, V., Gracio, J. & Buehler, M.J. 2014 Tuning heterogeneous poly(dopamine) structures and mechanics: in silico covalent cross-linking and thin film nanoindentation. *Soft Matter* **10**, 457-464. (doi:10.1039/c3sm51810h).

[10] Stukowski, A. 2010 Visualization and analysis of atomistic simulation data with OVITO-the Open Visualization Tool. *Model. Simul. Mater. Sci. Eng.* **18**, 1-7. (doi:10.1088/0965-0393/18/1/015012).